Theory of nonlinear whispering-gallery-mode dynamics in surface nanoscale axial photonics microresonators

Alena Yu. Kolesnikova* and Ilya D. Vatnik
Novosibirsk State University, 2 Pirogova Street, Novosibirsk 630090, Russia

(Received 20 March 2023; accepted 5 September 2023; published 13 September 2023)

We present a comprehensive model describing the Kerr nonlinear dynamics of an electric field in a cylindrical microresonator with a small effective radius variation, known as a surface nanoscale axial photonics (SNAP) device. The proposed system of equations for coupled azimuthal modes takes into account full azimuthal dispersion as well as the impact of the radiation source on the microresonator parameters. The model comprises coupling coefficients determined experimentally and appears to be a powerful tool for studying nonlinear effects, including the generation of axial-azimuthal modes and optical frequency comb generation in SNAP devices. We highlight the features of nonlinear dynamics that are specific to the SNAP platform and illustrate the power of the proposed model with optimization of the coupling point of the light source, getting two-orders-of-magnitude improvement for the nonlinear threshold.

DOI: 10.1103/PhysRevA.108.033506

I. INTRODUCTION

Optical microresonators are currently pushing forward research in photonics in many directions. Due to their small mode volume and high quality factors, microresonators are an excellent test bed for probing nonlinear and quantum optics problems [1]. For instance, the optical frequency combs (OFCs) generated in microcavities unlock spectroscopic devices of exceptional precision [2]. Depending on the free spectral range of the comb, different applications are preferred: While high-repetition-rate OFCs are appreciated in optical communications and subterahertz generation, spectroscopy applications such as dual-comb spectroscopy may benefit from lower-repetition-rate OFCs [3].

There is a microresonator platform possibly facilitating low-repetition-rate comb generation that is called surface nanoscale axial photonics (SNAP) [4]. The platform exploits a cylindrical microresonator, frequently made of standard optical fiber with removed plastic cladding, with introduced small-scale radius variations (see Fig. 1). The variation of the effective radius (the product of the cladding radius r and its refractive index n) plays the role of an optical potential that constrains whispering gallery modes (WGMs), splitting each azimuthal mode with a certain number of azimuthal maxima into a series of axial modes (with different numbers of axial nodes). The precise design of tiny variations reduces the spectral distance between adjacent axial resonances down to hundreds of megahertz [5], paving the way to a low-repetition frequency comb, while the high accuracy of the modifications may help in controlling the dispersion for efficient generation of the OFCs [6]. Moreover, if the radius variation is large enough, different series of axial modes overlap making an ultrawide low-repetition-rate OFC with hundreds of lines feasible [7].

However, no nonlinear process has yet been observed in such microresonators, as most experimental attempts have concentrated on bottlelike resonators [8–10]. Those are similar to SNAP cavities but have considerably larger radius variations and thus lower mode volumes as well as a much larger free spectral range for axial modes, and so they are not suitable for low-repetition-rate OFCs. Thus special attention should be paid to modeling nonlinear properties in SNAP cavities to reveal the possible obstacles that may prevent the observation of nonlinear processes.

At first glance, the solution is the well-established paradigm of the generalized Lugiato-Lefever (LL) equation [11], which was successfully implemented for bottlelike resonators [8,12,13]. Though the SNAP cavities imply small radius variations such that a coupling element, launching light into the cavity, may noticeably disturb the optical potential [14], the LL-based models presented earlier are not applicable.

Indeed, in most realized SNAP cavities, the tapered optical fiber is used as a coupling element, and it is put in direct physical contact with the microresonator. As a result, two noticeable effects arise [15]. The first is that the taper introduces a considerable variation in the effective radius that leads to a shift of the resonant frequencies of the axial modes. In this case, the shift depends on the position of the taper z_0 along the microresonator axis z; so each axial mode experiences different detuning because of the taper. This brings additional dispersion having an impact on the nonlinear dynamics.

The second experimentally observed effect brought by the taper is the introduction of additional scattering losses that are not related to the escape of radiation into the taper [15,16]. The different axial modes experience different additional losses because of the taper and thus must have different decay times, which also complicates the nonlinear dynamics.

*a.kolesnikova@g.nsu.ru

 ©2023 American Physical Society

Since the taper has a strong influence on the nonlinear mode generation, it is extremely important to include these effects in the model.

The impact of the taper has been accounted for in the model based on the stationary Schrödinger equation describing axial mode distribution [14]. The model is useful for designing the necessary effective radius variations. In Refs. [6,17] this model was dynamically extended to describe the evolution of a single azimuthal mode, as well as for two azimuthal modes [18]. However, this extension does not account for an arbitrary number of azimuthal modes. Moreover, uncertainty in the normalization of the wave functions of axial modes in Ref. [14] does not allow one to find the exact relationship between the coupling parameters and experimentally measured values in the dynamical model. Therefore this model is hardly applicable to determine the real threshold values of the power of nonlinear generation.

In our recent work [19] we presented a mathematical model of nonlinear dynamics of axial-azimuthal modes in a microresonator coupled to a source. However, this model does not comprise the real experimental parameters either, thus not allowing us to judge the feasibility of the optical frequency comb in the experiment. Thus none of the existing models makes it possible to describe the nonlinear interaction of axial-azimuthal modes in SNAP at a quantitative level.

In this paper, we present a system of equations derived from first principles that is a complete, generalized model for describing the SNAP system. The dynamical model includes the nonlinear interaction of azimuthal modes, the total dispersion of axial-azimuthal modes (including material dispersion), and the influence of the radiation source on the propagation of modes in the microcavity. Using the proposed model, we expose the importance of the impact of the coupling element on the nonlinear threshold and demonstrate that large axial extension of SNAP modes allows optimization of a coupling point, reducing the threshold from a hundred watts to experimentally achievable values of the order of hundreds of milliwatts.

II. MATHEMATICAL MODEL

A. System of nonlinear equations for the dynamics of azimuthal modes

To derive the model, we start with Maxwell's equations and obtain the wave equation under the condition of propagation of radiation in homogeneous isotropic dielectric matter. We neglect $(\vec{\nabla}\vec{E})$ due to the smallness of the nonlinearity and consider only a linear polarization [either a transverse magnetic (TM) or a transverse electric (TE) mode]:

$$\Delta E(\vec{r},\omega) + n(\omega)^2\frac{\omega^2}{c^2}E(\vec{r},\omega) = -\mu_0\omega^2(P_{\mathrm{NL}}(\vec{r},\omega) + P_p(\vec{r},\omega)). \tag{1}$$

For SNAP cavities, small effective radius variations Δr_{eff} are supposed; so $\Delta r_{\mathrm{eff}} \ll r_{0_{\mathrm{eff}}}$, where $r_{0_{\mathrm{eff}}}$ is the undisturbed effective radius of the cylinder. In this approximation, the electric field either in the time or frequency domain is represented as an expansion into the series of azimuthal modes of an infinite cylindrical resonator:

$$E(\vec{r},t) = \sum_m A_m(z,t)\exp(i\omega_m t)e_m(r,\varphi) + \text{c.c.},$$
$$E(\vec{r},\omega) = \sum_m A_m(z,\Delta\omega_m)e_m(r,\varphi) + \text{c.c.} \tag{2}$$

Here, $A_m(z,t)$ is the slowly varying amplitude of the azimuthal mode containing information about the dynamic of axial modes along the z axis, $\Delta\omega_m = \omega - \omega_m$, and ω_m is the resonance frequency of the azimuthal mode. $e_m(r,\varphi)$ is the spatial transverse field distribution of an azimuthal mode with azimuthal number m with $\max|e_m(r,\varphi)| = 1$. A detailed description of the modes of an infinite cylindrical microresonator is given in Appendix A.

Starting with Eq. (1), we sequentially derive a linear stationary equation for WGMs, then take into account the radiation source, and then take into account Kerr nonlinear terms. The detailed derivation of the dynamic model can be found in Appendix B. As a result, we have obtained a system of nonlinear dynamic equations of azimuthal modes coupled through the Kerr nonlinearity:

$$i\frac{\partial A_m}{\partial t} - \frac{\omega_m}{2k_m^2K_m}\frac{\partial^2A_m}{\partial z^2} - \frac{\omega_m}{K_m}\frac{\Delta r_{\mathrm{eff}}(z)}{r_{0_{\mathrm{eff}}}}A_m + i\Gamma A_m - \frac{3\omega_m\chi^{(3)}}{K_m 2n_m^2S_m}F_m(\vec{A}) + D_m f_p(z)A_m = \sqrt{\frac{P_{\mathrm{in}}}{\varepsilon_0 n_m^2 S_m}}C_m f_p(z)e^{i(\omega_p-\omega_m)t}, \tag{3}$$

where the nonlinear term $F_m(\vec{A})$ is determined by Eq. (C4).

Here, $k_m = \frac{\omega_m n(\omega_m)}{c}$, $K_m = 1 + \frac{\omega_m}{n_m}\frac{\partial n}{\partial\omega}(\omega_m)$ is the coefficient of material dispersion, $n_m = n(\omega_m)$ is the refractive index, $S_m = \int|e_m(r,\varphi)|^2d^2r$ is the effective mode cross section, $\chi^{(3)}$ is the nonlinear susceptibility, Γ is the internal losses of the microresonator, P_{in} is the pump power, and ω_p is the pump frequency.

Here, $f_p(z)$ is the normalized spatial distribution of the source radiation $[\int f_p(z)dz = 1]$, which for the case of the thin taper with a waist of a few micrometers can be considered as delta shaped: $\delta(z - z_0)$, where z_0 is an axial coordinate of the contact between the taper and the cavity.

Coupling parameters C_m and D_m are defined as

$$C_m = \frac{\chi\omega_p^2}{K_m 2\omega_m n_m}\sqrt{\frac{\varepsilon_0}{P_{\mathrm{in}}S_m}}\int E_p(r,\varphi)e_m^*d^2r,$$
$$D_m = -\frac{\omega_m}{K_m r_{0_{\mathrm{eff}}}}\int\Delta r_t(r,\varphi)e_m^*d^2r \tag{4}$$

determined by the overlap integral of the guided mode of a taper and transverse distribution of the whispering gallery mode at the cross section of the cylinder. C_m contains information about the pump power and coupling strength. The real part of D_m leads to an additional effective radius variation, and the imaginary part contributes to the losses experienced by the mode owing to the taper. Importantly, the parameters C_m and D_m are not dependent on the position of the coupling element z_0. Note that coefficients C_m and D_m have different dimensions

compared with those introduced in the earlier version of the stationary model based on the Schrödinger equation [14,15].

The system of equations (3) is a complete model that describes the dynamics of interacting modes in a cylindrical microcavity coupled to an exciting element. To use the model, coupling parameters D_m and C_m should be specified. Calculating the integrals in Eqs. (4) in the general case might be meaningless, as the mode distribution within a coupling element usually is not controlled precisely. Therefore it is necessary to relate D_m and C_m with quantities determined in the experiment, which will be done in the next section.

B. Determining the coupling parameters C_m and D_m

To link C_m and D_m with observables, one may deduce the transmission spectrum $T(\lambda)$ of the microresonator-taper system, which is an experimentally measurable function, from the system (3). For this, one can reduce the model (3) to the simple equation for coupling between the guided mode of the taper and a particular whispering gallery mode [20,21]. Note that the taper is assumed to be a single mode. Within this coupled-mode theory, the transmission spectrum $T(\lambda, \delta_0, \delta_c)$ is defined, giving a way to gather the coupling strength coefficient δ_c and the losses δ_0 experienced by the whispering gallery mode in an experiment (see Appendix D).

Since measurements of the transmission spectrum are performed at low powers, shrinking (3) to the form of Eq. (D1) may be done for the linear case. If a single azimuthal-axial mode with the azimuthal number m and axial number q is excited, the amplitude is represented in the form $A_m(z,t) = a_m(t)e^{i(\omega_p-\omega_m)t}Z_q(z)$ with normalization $\max Z_q(z) = 1$, and the dynamical equation is reduced to

$$i\frac{\partial a_m}{\partial t}Z_q - (\omega_p-\omega_m)a_m Z_q - \frac{\omega_m}{2k_m^2K_m}\frac{\partial^2 Z_q}{\partial z^2}a_m - \frac{\omega_m}{K_m}\frac{\Delta r_{\text{eff}}(z)}{r_{0_{\text{eff}}}}a_m Z_q + i\Gamma Z_q a_m + D_m f_p(z) Z_q a_m = \sqrt{\frac{P_{\text{in}}}{\varepsilon_0 n_m^2 S_m}}C_m f_p(z). \tag{5}$$

Multiplying Eq. (5) by $Z_q(z)$ and integrating over z, one gets

$$i\frac{\partial a_m}{\partial t}L_q - (\omega_p-\omega_m)L_q a_m + D_m Z_q^2(z_0)a_m - \int\left(Z_q\frac{\omega_m}{2k_m^2K_m}\frac{\partial^2 Z_q}{\partial z^2} + Z_q\frac{\omega_m}{K_m}\frac{\Delta r_{\text{eff}}(z)}{r_{0_{\text{eff}}}}Z_q\right)dz a_m + i\Gamma L_q a_m = \sqrt{\frac{P_{\text{in}}}{\varepsilon_0 n_m^2 S_m}}C_m Z_q(z_0). \tag{6}$$

Here, $L_q = \int Z_q^2(z)dz$ is the effective mode length.

The term with the integral can be represented as $\langle q|\hat{H}|q\rangle$, where $\hat{H} = \frac{\omega_m}{2k_m^2K_m}(\frac{\partial^2}{\partial z^2} + 2k_m^2\frac{\Delta r_{\text{eff}}(z)}{r_{0_{\text{eff}}}})$. According to the stationary Schrödinger equation (B6), this matrix element expresses the energy of the mode with the number q:

$$\langle q|\hat{H}|q\rangle = E_q L_q = (\omega_m - \omega_{m,q})L_q. \tag{7}$$

As the source detuning $\Delta\omega_{m,q} = \omega_p - \omega_{m,q} - \Omega$ [$\Omega = \text{Re}(D_m)Z_q^2(z_0)/L_q$], we get

$$i\frac{\partial a_m}{\partial t} - \Delta\omega_{m,q}a_m + i\Gamma a_m + i\,\text{Im}(D_m)Z_q^2(z_0)/L_q a_m = \sqrt{\frac{P_{\text{in}}}{\varepsilon_0 n_m^2 S_m}}C_m Z_q(z_0)/L_q. \tag{8}$$

Equaling each term in Eqs. (D1) and (8), we get the relationship between C_m and D_m and experimentally observable δ_0, δ_c, and Ω, which is the resonance frequency shift owing to additional effective radius variations introduced by the taper:

$$\text{Re}(D_m) = \Omega\frac{L_q}{Z_q^2(z_0)},$$
$$\text{Im}(D_m) = (\delta_0 + \delta_c - \Gamma)\frac{L_q}{Z_q^2(z_0)}, \tag{9}$$
$$C_m = -i\left(\delta_c\frac{L_q}{Z_q^2(z_0)}\right)^{\frac{1}{2}}.$$

C. Measurement of coupling parameters: An example

As per Eqs. (9), to find C_m and D_m within the proposed model, one should not only define δ_c and δ_0 from a transmission spectrum of a cavity-taper system, but also know the mode intensity at the coupling point $Z_q^2(z_0)$ and the effective length L_q for the azimuthal-axial cavity mode under test. Fortunately, it can be derived from measurements of δ_c and δ_0 for different excitation points z_0. Indeed, from Eqs. (9) it follows that

$$\Omega(z_0) = \text{Re}(D_m)\frac{Z_q^2(z_0)}{L_q},$$
$$\delta_c(z_0) = |C_m|^2\frac{Z_q^2(z_0)}{L_q}, \tag{10}$$
$$\delta_0(z_0) = (\text{Im}(D_m) - |C_m|^2)\frac{Z_q^2(z_0)}{L_q} + \Gamma.$$

Interestingly, δ_0 and δ_c depend on z_0 and are proportional to the axial mode spatial distribution $Z_q^2(z)$. Firstly, this relation was revealed in Ref. [14] with the emphasis on transmission spectrum properties. The experimental dependencies $\delta_c(z_0)$ and $\delta_0(z_0)$ for a mode q, derived from the transmission spectrum $T(z_0, \lambda)$ at different positions of the taper along the z axis (see Appendix D) thus can be fitted to get C_m, D_m, and Γ.

We demonstrate the feasibility of the method, carrying out measurements of coupling parameters for a 1-μm taper that is in physical contact with a SNAP cavity based on a piece of standard optical fiber (SMF-28) with $r_0 = 62.5$ μm. To localize modes along the z axis, we introduced a bell-shaped effective radius variation Δr_{eff} with local heating by a CO_2 laser [4].

The measured spectrogram $T(z_0, \lambda)$ represents spatial distribution of the axial modes with numbers $q = 0\cdots3$ (see Fig. 2). The spectral resolution was not worse than 5 MHz. The first consequence of Eqs. (10) is that the linewidth of the resonance $\delta_0 + \delta_c$ is maximal at the mode antinodes. The

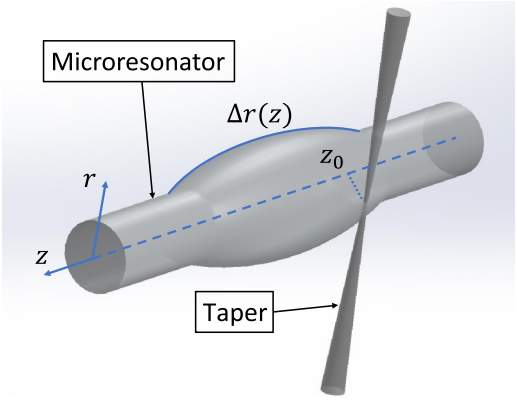

FIG. 1. SNAP platform: a cylindrical microresonator with an effective radius variation based on standard optical fiber coupled to an input-output taper.

second is that the typical resonance width for a mode with a lower number q is larger, as the effective mode length L_q is smaller.

We chose the first axial mode with $q = 0$ [see Fig. 3(a)] to determine the coupling parameters $\delta_c(z_0)$ and $\delta_0(z_0)$. For this mode, one can suppose a Gaussian function for the axial distribution $Z_0^2(z)$ and so decrements $\delta_c(z) = |C_m|^2/L_0 e^{-(z-a)^2/w^2}$ and $\delta_0(z) = (\mathrm{Im}(D_m) - |C_m|^2)/L_0 e^{-(z-a)^2/w^2} + \Gamma$ [see Fig. 3(b)]. By fitting the two lines $\delta_c(z_0)$ and $\delta_0(z_0)$ jointly with Gaussian shapes, we determined coupling parameters $\mathrm{Im}(D_m) = (7.6 \times 10^4) \pm (1.7 \times 10^3)$ m/s and $|C_m|^2 = (2.1 \times 10^4) \pm (5.3 \times 10^2)$ m/s. The upper bound for internal losses is determined as $\Gamma < 30\ \mu\mathrm{s}^{-1}$, defined by the resolution of the optical spectral analyzer.

Defining $\mathrm{Re}(D_m)$ by fitting equations jointly (10) is problematic because of the low absolute resolution of the optical spectrum analyzer used. Nevertheless, one can estimate the shift of the resonant frequency $\Omega = -\Lambda\omega_m/\lambda_m = \mathrm{Re}(D_m)Z_0^2(z_0 = 0)/L_0$ [see Fig. 3(b)], finding $\mathrm{Re}(D_m) = -9.7 \times 10^4$ m/s.

It should be noted that the dependence of the width and shift of axial resonances and their connection with the coupling parameters has already been studied in Ref. [14]. In this paper, the coefficients D and $|C|^2$ are presented, which, in essence, are also coupling parameters determined by the

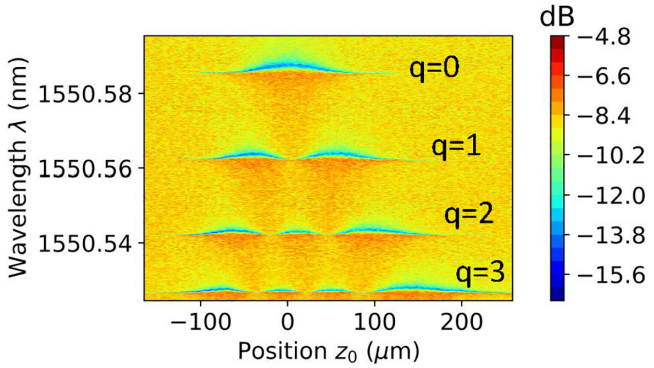

FIG. 2. The measured spectrogram $T(z_0, \lambda)$ of the SNAP cavity with a bell-shaped effective radius variation.

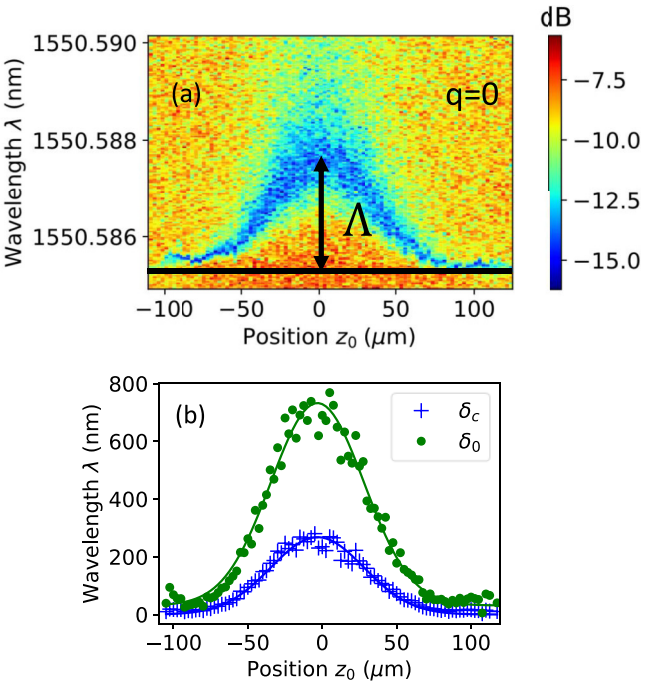

FIG. 3. (a) The spectrogram of the SNAP system: the axial mode with $q = 0$. (b) The approximation of the experimental decrements δ_c and δ_0.

overlap integral of the taper and resonator modes and thus proportional to the parameters D_m and C_m defined in the current model. However, the uncertainty in the normalization of the wave functions of axial modes in Ref. [14] does not allow using parameters D and $|C|^2$ in the dynamical model or determining the nonlinear thresholds.

The dependence of the linewidth $\delta = \delta_c + \delta_0$ and resonance shift Ω on the taper position may drastically affect the nonlinear mode dynamics. Indeed, in accordance with Eqs. (10), for the given coupling point z_0, different axial modes experience different linewidth broadening and resonance shifts since the mode amplitudes differ $[Z_{q_1}(z_0) \neq Z_{q_2}(z_0)]$, as do the effective lengths $(L_{q_1} \neq L_{q_2})$. Thus modes with smaller effective lengths are highly disturbed, with the resonance width being orders of magnitude larger than the resonance width of well-extended modes. The uneven shift of the resonant frequencies leads to additional axial mode dispersion with alternating sign. Given the experimental example under consideration with $\mathrm{Re}(D_m) = -9.7 \times 10^4$ m/s, such an alternating dispersion may be of the order of dozens of megahertz. Both these effects should significantly change the nonlinear dynamics of axial modes compared with the results presented in Ref. [13]. A detailed study of these dynamics will be published elsewhere.

III. OPTIMIZING THE NONLINEAR THRESHOLD

Dependence of the decrements δ_0 and δ_c on the contact point z_0 along the axis of the cylinder is a fundamental feature of SNAP microresonators that grants control over both intrinsic and loaded quality factors (Q factors). In contrast,

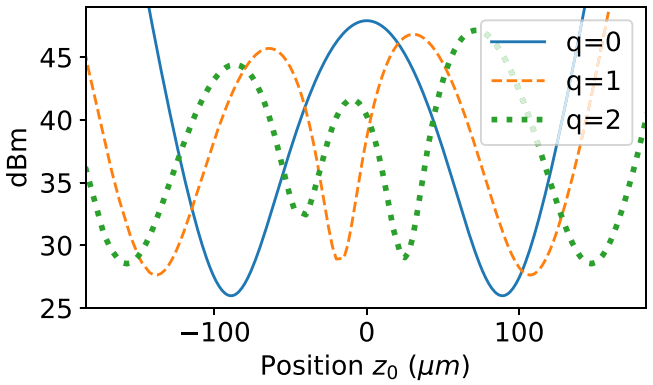

FIG. 4. Nonlinear threshold $P_{\text{in}}^{\text{th}}$ approximated for different coupling points z_0 for different axial modes of the SNAP cavity under study. The taper waist is assumed to be 2 μm.

ideal spherical microresonators have a symmetry that imposes identical decrements for any contact point.

The control over quality factors, in turn, helps in achieving nonlinear generation. From a simple coupling model, the power threshold for observing nonlinear effects may be derived using the coupling decrements [22]:

$$P_{\text{in}}^{\text{th}} = \frac{4\varepsilon_0 K_m n_m^4 V_{m,q}^2}{3\omega_m \chi^{(3)} V_{mm,qq}} \frac{\delta^3}{\delta_c}. \tag{11}$$

Here, $V_{mm,qq} = S_{mmmm} \int Z_q^4(z)dz$.

Thus, in SNAP microresonators, the nonlinear threshold also depends on the coupling point z_0 and might be optimized. Taking into account the dependencies $P_{\text{in}}^{\text{th}} \sim \frac{(\delta_0(z_0)+\delta_c(z_0))^3}{\delta_c(z_0)}$ and Eqs. (10), we have found that the minimum threshold is reached when coupling occurs at the point z_0 defined by $Z_q^2(z_0) = \frac{\Gamma L_q}{2\,\text{Im}(D_m)}$.

The optimized power threshold is then equal to

$$P_{\text{in}}^{(\text{min})} = \frac{9\varepsilon_0 K_m n_m^4 V_{m,q}^2}{\omega_m \chi^{(3)} V_{mm,qq}} \frac{\Gamma^2\,\text{Im}(D_m)}{|C_m|^2}. \tag{12}$$

To illustrate the capabilities of the coupling optimization, we determine the minimum power threshold for the axial mode with $q = 0$ within the experimentally studied SNAP cavity [see Fig. 3(a)]. While coupling at the maximum of the mode distribution would require $P_{\text{in}} = 61$ W to obtain the nonlinear threshold, the optimized coupling point yields threshold power as low as $P_{\text{in}}^{(\text{min})} = 396$ mW. Nevertheless, constraints may make it difficult to take advantage of such a threshold. Indeed, the point z_0 corresponding to the minimal power $P_{\text{in}}^{(\text{min})}$ is three mode widths away from the center of the mode (see Fig. 4), thus yielding tiny, but still not equal, coupling parameters δ_c and δ_0. Thus the corresponding resonance in the transmission spectrum might be hardly detectable with a moderate-resolution spectrometer [according to (D2)]. With this, the strong dependence of the threshold on z_0 demands sufficient accuracy of the z_0 setting.

Generally, for each axial mode with an axial number q there are $2(q+1)$ points along z in which the threshold power $P_{\text{in}}^{\text{th}}(z_0)$ achieves the local minimum. In the approximation $\int Z_q^2(z) f_p(z)dz = Z_q^2(z_0)$ all minima are equal and are defined by Eq. (12). In a real system, the taper has a finite size, and the threshold value (12) must be derived more accurately, giving minima at the points where the axial mode distribution function changes slowly. In other words, the minimum will be reached at the edges of the mode distributions (see Fig. 4). At other local minimum points, the threshold is higher since the mode distribution function changes faster, and the overlap integral with the source of the finite size is larger.

This is an unexpected result. As the taper introduces significant additional losses, the undercoupling regime usually is realized [15]. Therefore one can intuitively assume that the minimum threshold will be reached at the maximum of the mode distribution. However, accounting for the dependence of the losses on the taper position z_0 shows the assumption to be wrong: The lowest nonlinear threshold is reached just in the opposite situation, when the taper is put in contact with the cavity at the very edge of the mode.

IV. CONCLUSION

We present a complete, generalized model describing light evolution in Kerr nonlinear cylindrical microresonators with slight radius variations disturbed by a coupling element. The model comprises nonlinear Kerr interactions between axial-azimuthal modes and takes into account disturbances introduced by the coupling element, which may drastically change the light dynamics. We also propose a method to experimentally determine the coupling parameters. It is shown that the coupling element may introduce determinant losses to a mode, as well as additional alternating axial dispersion, and thus must be taken into account while analyzing nonlinear threshold and dynamics in SNAP resonators. Within the proposed model, we reveal possibilities for minimization of the nonlinear Kerr threshold by choosing the proper position of a thin taper exciting a mode. For a particular SNAP cavity made of SMF-28 fiber with a mode length of 80 μm, optimization decreases the threshold from 61 W down to 0.4 W. The model may become a powerful tool for studying the nonlinear interactions of azimuthal-axial modes in disturbed cylinders.

ACKNOWLEDGMENT

The study was supported by the Russian Science Foundation (Grant No. 22-12-20015) and by the Government of the Novosibirsk Region [23].

APPENDIX A: MODES OF THE INFINITE CYLINDER

It is known that modes of an infinite cylinder with no radius variations $\Delta r = 0$ may have two different polarizations [24], TE and TM. In the case of the TM mode, the electric field vector has only one component, E_z. For the TE mode, we neglect the component of the electric field E_φ in the case of $m \gg 1$, since it is much smaller than component E_r. Thus we can assume that TE and TM modes have linear polarization and (1) has the same form for the TE and TM modes. The electric field can then be represented as

$$E(\vec{r}, \omega) = R(\sqrt{k^2 - \beta^2} r) e^{im\varphi} e^{i\beta z}, \tag{A1}$$

where $k = \omega n/c$.

We solve the following equation:

$$(\Delta_T + (k^2 - \beta^2))R(\sqrt{k^2 - \beta^2}r)e^{im\varphi} = 0. \quad \text{(A2)}$$

In the case of $\beta = 0$, the solution of (A2) corresponds to a distribution of the azimuthal-radial mode at the infinite cylinder $e_{m,p}(r, \varphi) \equiv R(k_{m,p}r)e^{im\varphi}$, where $R(k_{m,p}r) = \mathrm{Ai}(-(2/m)^{1/3}(T_{m,p}r/\tilde{a} - m))$, $\mathrm{Ai}(x)$ is the Airy function, $T_{m,p}$ is the pth zero of the mth Bessel function, $\tilde{a} = r_0 + P/\gamma$, $\gamma = \sqrt{n^2 - 1}\omega_{m,p}/c$, $P = 1$ for TE modes, and $P = 1/n^2$ for TM modes [24].

Here, $k_{m,p} = \omega_{m,p}n(\omega_{m,p})/c$, $\omega_{m,p}$ is the frequency of the azimuthal-radial mode of an ideal cylindrical microresonator with no radius variations, and m and p are the azimuthal and radial quantum numbers, respectively. $\omega_{m,p}$ is determined from the characteristic equation (A3) in Ref. [24]. It is noteworthy that the expression for resonant frequencies $\omega_{m,p}$ may not only take into account the geometric mode dispersion as in Ref. [24], but also comprise the material dispersion, if we assume $n \equiv n(\omega_{m,p})$ and solve the implicit equation (A3).

In this paper, we analyze only one radial mode and omit the index p for simplicity. Generally, the proposed model can be easily extended to take into account other radial modes.

APPENDIX B: DERIVATION OF A SYSTEM OF NONLINEAR EQUATIONS FOR THE DYNAMICS OF AZIMUTHAL MODES

1. Stationary model for a single azimuthal mode

At the first stage, we take into account a radius variation and find the stationary equation for a single azimuthal-radial mode represented in the following form:

$$E(\vec{r}) = A_m(z, \omega)R(\sqrt{k^2 - \beta^2}r)e^{im\varphi}. \quad \text{(B1)}$$

The expansion (B1) is valid for small radius variations $\Delta r(z)$: $\Delta r(z) \ll r_0$, where r_0 is an undisturbed radius of the cylinder. We substituted the expression for the field into (1) in the linear regime and divided the equation into axial and transverse parts:

$$(\Delta_T + (k^2 - \beta^2))R(\sqrt{k^2 - \beta^2}r)e^{im\varphi}A_m(z, \omega) + \left(\frac{\partial^2}{\partial z^2} + \beta^2\right)A_m(z, \omega)R(\sqrt{k^2 - \beta^2}r)e^{im\varphi} = 0. \quad \text{(B2)}$$

In the first-order approximation for the amplitude $A_m(z)$, in the presence of an effective radius variation for $m \gg 1$ the wave vector has a small component β directed along the axis z, such that $\beta \ll k_m$. In this case, we can assume that the characteristic equation for frequencies changed up to replacement $\sqrt{k^2 - \beta^2} \to k_m$ and β can be found from the following expression [4]:

$$\frac{\omega_m n(\omega_m) r_0}{c} = (r_0 + \Delta r(z))\sqrt{\frac{\omega^2 n(\omega)^2}{c^2} - \beta^2}. \quad \text{(B3)}$$

We expand $\omega^2 n^2(\omega)$ near ω_m and r_0 to the first order, taking into account the dependence of the refractive index $n(\omega) \equiv n(\omega, r(z))$ on the coordinate resulting from the introduction of a radius variation:

$$\beta^2 = 2k_m^2\left(\frac{\Delta r(z)}{r_0} + \frac{\Delta n(z)}{n_m} + K_m\frac{\Delta\omega_m}{\omega_m}\right). \quad \text{(B4)}$$

Here, $\Delta r(z)$ and $\Delta n(z)$ determine the effective radius variation.

In this case, the transverse part in Eq. (B2) is equal to the zero, according to Eq. (A2), and we receive the equation for a slowly varying amplitude of the azimuthal mode:

$$\frac{\partial^2 A_m(z, \omega)}{\partial z^2} + \beta^2 A_m(z, \omega) = 0. \quad \text{(B5)}$$

Then, we substitute β in Eq. (B5) with (B4) and obtain the Schrödinger equation describing the stationary distribution of the axial-azimuthal modes and their resonance frequencies.

$$\frac{\partial^2 A_m(z, \omega)}{\partial z^2} + V_m(z)A_m(z, \omega) = E_m A_m(z, \omega). \quad \text{(B6)}$$

Here, the potential is determined by the effective radius variation $V_m(z) = 2k_m^2\frac{\Delta r_{\mathrm{eff}}(z)}{r_{0_{\mathrm{eff}}}}$, where $\frac{\Delta r_{\mathrm{eff}}(z)}{r_{0_{\mathrm{eff}}}} = \frac{\Delta r(z)}{r_0} + \frac{\Delta n(z)}{n_m}$. The resonant frequencies correspond to the energy levels in the potential and are related as follows: $E_m = -2k_m^2\frac{\Delta\omega_m}{\omega_m}K_m$.

Equation (B6) is virtually the same as the equation obtained in Ref. [4]. The difference in the current version of the equation is that it takes into account the material dispersion of azimuthal modes through the coefficient K_m. Despite the smallness of the correction $K_m - 1 \ll 1$, it might be crucial for considering the interactions between different azimuthal modes, as it imposes additional azimuthal dispersion as well as dissimilar axial free spectral ranges for different azimuthal modes for the same $\Delta r_{\mathrm{eff}}(z)$.

In order to take into account the internal losses in the microresonator medium, one can modify the energy definition as follows: $E_m = -2k_m^2\frac{\Delta\omega_m}{\omega_m}K_m + i\Gamma$ [14]. Here, losses Γ may in principle depend on azimuthal or radial quantum numbers and are defined by the intrinsic losses within the cylinder media as well as by the surface quality.

2. Dynamical model with a source and nonlinearity

To generalize the approach presented in the previous section to the case of an arbitrary number of azimuthal modes, the field should be represented as (2). Substituting the field in the form of (2) into Eq. (1), and taking into account Eqs. (A2) and (B4), one obtains

$$\sum_m\left(\frac{\partial^2}{\partial z^2} + 2k_m^2\left(\frac{\Delta r_{\mathrm{eff}}(z) + \Delta r_t(\vec{r})}{r_{0_{\mathrm{eff}}}} + K_m\frac{\Delta\omega_m}{\omega_m}\right) - i\Gamma\right) \times A_m(z, \omega)e_m(r, \varphi) = -\frac{\chi^{(3)}\omega^2}{c^2}E^3(\vec{r}, \omega) - \frac{\chi\omega^2}{c^2}E_p(\vec{r}, \omega). \quad \text{(B7)}$$

We consider the Kerr nonlinearity $P_{\mathrm{NL}} = \epsilon_0\chi^{(3)}E^3$, as the SNAP cavities are usually assumed to be on silica. The pump field $E_p(\vec{r}, t) = E_p(\vec{r})e^{i\omega_p t}$, where ω_p is the pump frequency.

Importantly, we here introduce an additional term $\Delta r_t(\vec{r})$ to emphasize the additional effective radius variation that may appear in the presence of a coupling element, for instance, a

taper being in contact with the cavity [14,15]. Complex effective radius variation $\Delta r_t(\vec{r}) = \Delta r_t'(\vec{r}) - i\Delta r_t''(\vec{r})$ accounts both for the change in the structure of the microcavity eigenmodes and for additional losses.

To proceed to the dynamic equation, we take the inverse Fourier transform of (B7) and take out of the brackets the coefficient $2k_m^2 K_m/\omega_m$.

$$\sum_m 2\omega_m K_m n_m^2 \left(i\frac{\partial}{\partial t} - \frac{\omega_m}{2k_m^2 K_m}\frac{\partial^2}{\partial z^2} - \frac{\omega_m}{K_m}\frac{\Delta r_{\text{eff}}(z)}{r_{0_{\text{eff}}}} - \frac{\omega_m}{K_m}\frac{\Delta r_t(\vec{r})}{r_{0_{\text{eff}}}} + i\Gamma \right) A_m(z,t)e_m = -e^{-i\omega_m t}\chi^{(3)}\frac{\partial^2 E^3}{\partial t^2} + e^{i(\omega_p-\omega_m)t}\chi\omega_p^2 E_p(\vec{r}). \quad \text{(B8)}$$

Multiplying Eq. (B8) by e_m^* and integrating over the cross section of the cylinder, implying that modes with different azimuthal numbers are orthogonal, we obtain

$$i\frac{\partial A_m}{\partial t} - \frac{\omega_m}{2k_m^2 K_m}\frac{\partial^2 A_m}{\partial z^2} - \frac{\omega_m}{K_m}\frac{\Delta r_{\text{eff}}(z)}{r_{0_{\text{eff}}}}A_m + i\Gamma A_m + e^{-i\omega_m t}\frac{\chi^{(3)}\int e_m^*\frac{\partial^2 E^3}{\partial t^2}d^2r}{K_m 2\omega_m n_m^2 S_m} + D_m f_p(z)A_m = \sqrt{\frac{P_{\text{in}}}{\varepsilon_0 n_m^2 S_m}}C_m f_p(z)e^{i(\omega_p-\omega_m)t}. \quad \text{(B9)}$$

C_m and D_m are the coupling parameters and are expressed as (4).

Finally, with the simplification of the nonlinear term described in Appendix C, Eq. (B8) is rewritten in the form (3).

APPENDIX C: NONLINEAR TERM $F_m(\vec{A})$

To obtain a system of nonlinear equations from (B9), the nonlinear integral $\int e_m^*\frac{\partial^2 E^3}{\partial t^2}d^2r$ should be rewritten.

For this, the term E^3 may be expanded:

$$E^3 = \sum_{i,j,k}(\tilde{A}_i\tilde{A}_j\tilde{A}_k + 3\tilde{A}_i^*\tilde{A}_j\tilde{A}_k + 3\tilde{A}_i^*\tilde{A}_j^*\tilde{A}_k + \tilde{A}_i^*\tilde{A}_j^*\tilde{A}_k^*). \quad \text{(C1)}$$

Here, $\tilde{A}_i = A_i e^{i\omega_i t}e_i(r,\varphi)$.

Only a part of the terms constituting the sum will give a nonzero contribution to the integral $\int e_m^*\frac{\partial^2 E^3}{\partial t^2}d^2r$ because of oscillations in $e^{im\varphi}$:

$$\int e_m(r)e_i(r)e_j(r)e_k(r)e^{i\varphi(\pm i\pm j\pm k-m)}d^2r = 2\pi S_{mijk}, \quad \text{(C2)}$$

where $S_{mijk} = \int e_m(r)e_i(r)e_j(r)e_k(r)rdr$. The expression (C2) is valid for the case $\pm i \pm j \pm k - m = 0$.

It can be assumed that only terms with one conjugate amplitude will remain from the entire sum, provided that the number of azimuthal modes satisfies the condition $m \gg 1$ and also provided that the azimuthal modes have the same order (in order to define the condition $\pm i \pm j \pm k - m = 0$, only one index can have a negative sign, in other words, $i + j - k - m = 0$): $E^3 = 3\sum_{i,j,k}\tilde{A}_i\tilde{A}_j\tilde{A}_k^*$. We select from this sum all terms with $\tilde{A}_m$, which corresponds to two cases:

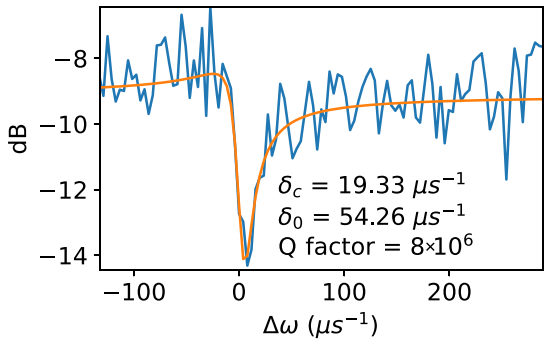

FIG. 5. An example of a measured transmission spectrum with the Fano profile approximation.

(1) For $i = m$, $j = m$, and $k = m$, we have $3|\tilde{A}_m|^2\tilde{A}_m$.

(2) For $i = m$ and $j \neq m$, we have $3\sum_{\substack{j=k\\ j\neq m}}(\tilde{A}_m\tilde{A}_j\tilde{A}_k^* + \tilde{A}_m\tilde{A}_j^*\tilde{A}_k)) = 6\sum_{j\neq m}(|\tilde{A}_j|^2\tilde{A}_m)$.

Thus we can rewrite the electric field in the form $E^3 = 3|\tilde{A}_m|^2\tilde{A}_m + 6\sum_{j\neq m}|\tilde{A}_j|^2\tilde{A}_m + 3\sum_{\substack{j\neq m\\ k\neq m\\ l}}\tilde{A}_j\tilde{A}_k\tilde{A}_l$. Substituting the decomposition of E^3 into the nonlinear integral in Eq. (B9), we obtain

$$\int e_m^*\frac{\partial^2 E^3}{\partial t^2}d^2r = -3\omega_m^2 F_m(\vec{A}), \quad \text{(C3)}$$

where

$$F_i(\vec{A}) = \left(S_{iiii}|A_i|^2 + 2\sum_{j\neq i}S_{jjii}|A_j|^2\right)A_i + \frac{(\omega_i + \Delta\omega_{ijkl})^2}{\omega_i^2}\sum_{\substack{j\neq i\\ k\neq i\\ l}}S_{ijkl}A_jA_kA_l^*e^{i(\Delta\omega_{ijkl})t}, \quad \text{(C4)}$$

where $\Delta\omega_{ijkl} = -\omega_i + \omega_j + \omega_k - \omega_l$ and $l = j + k - i$.

We have neglected the first and second derivatives of the amplitude $A_i(z,t)$, due to the smallness of $\chi^{(3)}$.

APPENDIX D: SIMPLE COUPLED-MODE EQUATION

Within the simple coupling model [20,21], the equation for a slowly varying mode amplitude in a linear regime with a spatial distribution $e(\vec{r})$ in a microcavity, where the field is defined as $E = (a(t)e(\vec{r})e^{i\omega_p t} + \text{c.c.})/2$, m is the mode number, and ω_p is the pump frequency [20], is as follows:

$$i\frac{\partial a(t)}{\partial t} - \Delta\omega a(t) + (\delta_0 + \delta_c)a(t) = iF. \quad \text{(D1)}$$

Here, $F = \sqrt{4P_{\text{in}}\delta_c/(\varepsilon_0\varepsilon V_{\text{eff}})}$, where P_{in} is the pump power, $V_{\text{eff}} = \int|e(\vec{r})|^2d^3r$ is the effective mode volume, $\max e_m(\vec{r}) = 1$, δ_c is the coupling strength coefficient, δ_0 is the losses experienced by the whispering gallery modes, and $\Delta\omega = \omega_p - \omega_{\text{res}}$ is the pump frequency detuning. The stationary solution of Eq. (D1) leads to the transmission spectrum T of the microresonator-taper system, which is an experimentally determined quantity, allowing us to determine the parameters δ_c and δ_0. Thus, in the case of a single-mode

coupling element, the transmission spectrum is described by the Fano resonance profile [14,25,26]:

$$|T|^2 = |S_0|^2 \left| e^{i\varphi_0} - \frac{2\delta_c}{i\Delta\omega + (\delta_0 + \delta_c)} \right|^2. \tag{D2}$$

Here, $S_0 = |S_0|e^{i\varphi_0}$ is the nonresonant transmission coefficient.

Figure 5 shows an example of such a transmission spectrum, measured for a particular axial-azimuthal mode in a SNAP microresonator with approximation with (D2). Approximation of the transmission spectrum makes it possible to determine the coupling parameters δ_0 and δ_c, which contain information about the overlap integrals of the radiation source field with the resonator mode and can be expressed in terms of the required parameters D_m and C_m.

[1] A. Pasquazi, M. Peccianti, L. Razzari, D. J. Moss, S. Coen, M. Erkintalo, Y. K. Chembo, T. Hansson, S. Wabnitz, P. Del'Haye, X. Xue, A. M. Weiner, and R. Morandotti, Micro-combs: A novel generation of optical sources, Phys. Rep. **729**, 1 (2018).

[2] R. Niu, M. Li, S. Wan, Y. R. Sun, S.-m. Hu, C.-l. Zou, G.-c. Guo, and C.-h. Dong, kHz-precision wavemeter based on reconfigurable microsoliton, Nat. Commun. **14**, 169 (2023).

[3] Y. Sugiyama, T. Kashimura, K. Kashimoto, D. Akamatsu, and F.-L. Hong, Precision dual-comb spectroscopy using wavelength-converted frequency combs with low repetition rates, Sci. Rep. **13**, 2549 (2023).

[4] M. Sumetsky and J. M. Fini, Surface nanoscale axial photonics, Opt. Express **19**, 26470 (2011).

[5] D. Bochek, N. Toropov, I. Vatnik, D. Churkin, and M. Sumetsky, SNAP microresonators introduced by strong bending of optical fibers, Opt. Lett. **44**, 3218 (2019).

[6] S. V. Suchkov, M. Sumetsky, and A. A. Sukhorukov, Frequency comb generation in SNAP bottle resonators, Opt. Lett. **42**, 2149 (2017).

[7] V. Dvoyrin and M. Sumetsky, Bottle microresonator broadband and low-repetition-rate frequency comb generator, Opt. Lett. **41**, 5547 (2016).

[8] X. Jin, X. Xu, H. Gao, K. Wang, H. Xia, and L. Yu, Controllable two-dimensional Kerr and Raman-Kerr frequency combs in microbottle resonators with selectable dispersion, Photonics Res. **9**, 171 (2021).

[9] M. Pöllinger and A. Rauschenbeutel, All-optical signal processing at ultra-low powers in bottle microresonators using the Kerr effect, Opt. Express **18**, 17764 (2010).

[10] S. Zhu, B. Xiao, B. Jiang, L. Shi, and X. Zhang, Tunable Brillouin and Raman microlasers using hybrid microbottle resonators, Nanophotonics **8**, 931 (2019).

[11] L. Lugiato, F. Prati, M. Gorodetsky, and T. Kippenberg, From the Lugiato–Lefever equation to microresonator-based soliton Kerr frequency combs, Philos. Trans. R. Soc. A **376**, 20180113 (2018).

[12] Y. V. Kartashov, M. L. Gorodetsky, A. Kudlinski, and D. V. Skryabin, Two-dimensional nonlinear modes and frequency combs in bottle microresonators, Opt. Lett. **43**, 2680 (2018).

[13] I. Oreshnikov and D. V. Skryabin, Multiple nonlinear resonances and frequency combs in bottle microresonators, Opt. Express **25**, 10306 (2017).

[14] M. Sumetsky, Theory of SNAP devices: basic equations and comparison with the experiment, Opt. Express **20**, 22537 (2012).

[15] D. L. P. Vitullo, S. Zaki, D. E. Jones, M. Sumetsky, and M. Brodsky, Coupling between waveguides and microresonators: the local approach, Opt. Express **28**, 25908 (2020).

[16] X. Jin, Y. Dong, and K. Wang, Selective excitation of axial modes in a high-Q microcylindrical resonator for controlled and robust coupling, Appl. Opt. **54**, 8100 (2015).

[17] M. Crespo-Ballesteros, A. B. Matsko, and M. Sumetsky, Optimized frequency comb spectrum of parametrically modulated bottle microresonators, Commun. Phys. **6**, 52 (2023).

[18] M. Crespo-Ballesteros and M. Sumetsky, Controlled Transportation of Light by Light at the Microscale, Phys. Rev. Lett. **126**, 153901 (2021).

[19] A. Y. Kolesnikova, S. V. Suchkov, and I. D. Vatnik, Frequency comb generation in SNAP fiber resonator based on axial-azimuthal mode interactions, Opt. Express **30**, 10588 (2022).

[20] M. L. Gorodetsky and V. S. Ilchenko, Optical microsphere resonators: optimal coupling to high-Q whispering-gallery modes, J. Opt. Soc. Am. B **16**, 147 (1999).

[21] A. Yariv, Universal relations for coupling of optical power between microresonators and dielectric waveguides, Electron. Lett. **36**, 321 (2000).

[22] T. Herr, K. Hartinger, J. Riemensberger, C. Y. Wang, E. Gavartin, R. Holzwarth, M. L. Gorodetsky, and T. J. Kippenberg, Universal dynamics of Kerr-frequency comb formation in microresonators, Nat. Photonics **6**, 480 (2012).

[23] https://rscf.ru/project/22-12-20015/.

[24] Y. A. Demchenko and M. L. Gorodetsky, Analytical estimates of eigenfrequencies, dispersion, and field distribution in whispering gallery resonators, J. Opt. Soc. Am. B **30**, 3056 (2013).

[25] M. F. Limonov, M. V. Rybin, A. N. Poddubny, and Y. S. Kivshar, Fano resonances in photonics, Nat. Photonics **11**, 543 (2017).

[26] Y. Lu, X. Zhu, J. Li, Y. Nie, M. Li, and Y. Song, Tunable oscillating Fano spectra in a fiber taper coupled conical microresonator, IEEE Photonics J. **11**, 2200807 (2019).